OPTIMAL TRAJECTORY PLANNING FOR MOBILE, MULTIBODY SYSTEMS

Eric Conrado de Souza, eric.csouza@yahoo.com
Marko Ackermann, mackermann@fei.edu.br
Av. Humberto de Alencar Castelo Branco, n.3972, Depto. de Engenharia Mecânica, Centro Universitário FEI, São Bernardo do Campo, SP, 09850-901, Brasil

Abstract. *In what follows, we present the dynamical model for a proposed class of mobile, multibody robotic systems which are able to steer themselves around on the plane. We employ open-loop optimal control towards trajectory generation for systems with unidirectional thrusting and compare to previously obtained results of systems with bidirectional thrusting capacity. We show through numerical trials that the gain of performance of the multibody systems over the rigid body with similar thrusting inputs is significantly greater when considering the unidirectional case.*

Keywords: *multibody systems, optimal control, mobile robotics*

1. INTRODUCTION

1.1 System Definition

Definition 1.1 (Mobile Multibody System, Souza and Maruyama (2010)) *Let the multibody system of Figure 1 be formed by N rigid bodies connected to each other through articulated joints in the form of an open chain and subject to, at most, N external forces f_i, and with up to $N-1$ joint torques T_j. Allowing the f_i to represent propulsion actuators, the system can be steered on the inertial space and freely position its center of mass.*

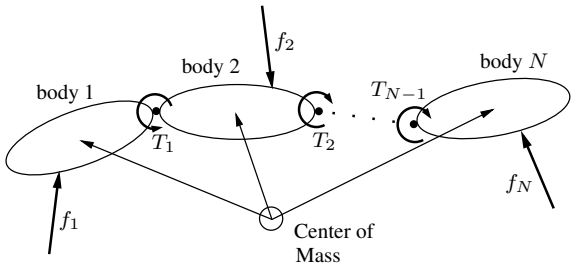

Figure 1. Mobile multibody system.

Systems of this class are simply kinematic chains composed of planar rigid bodies which are articulated by active hinges. Systems of the mentioned class pertain to a myriad of applications, ranging from underwater and space robotics to behavioral models for biomechanics research Ackermann and van den Bogert (2010). The above defined system differs from those considered in the literature, see e.g. Rui *et al.* (2000), Dubowsky and Papadopoulos (1993), in regard to the distribution of thrusters inputs: one in each system body, in contrast to a concentrated input structure. This property couples system translational and angular dynamics. Our motivation for the following investigation finds its origin in the practical problems of autonomous robotics. We employ open-loop optimal control towards trajectory generation for such systems as described next.

1.2 Problem Statement

Consider the rigid body system with two thrusters, as defined in the Appendix, which we henceforth refer to as the *reference system* or simply RS.

We intend to verify a gain of performance of the above multibody systems relative to the RS. The above class of multibody systems can be viewed as a partitioned rigid body where kinematical constraints were removed and becomes kinematically redundant, i.e., has more d.o.f. than the cartesian space. Our objective is to show superior multibody system performance by exploiting the breaking of these kinematical constraints or its inherent redundancy. In this regard, i.e., in the attempt to verify improvement of the multibody system performance over the RS, we carry out a numerical investigation to seek optimal trajectories which minimize a certain functional dependent on systems inputs only.

This study serves as a preliminary evaluation of system actuation capacity as attention is given to both bidirectional and unidirectional thrusting, defined by:

Bidirectional: $f_i \in [-1;1] \cdot f_{max}$,

Unidirectional: $f_i \in [0;1] \cdot f_{max}$.

One sought for conclusion of this study extension is that multibody systems outperform the RS even more pronouncedly when operating with unidirectional thrusting. Moreover, we carry out additional analysis to quantify the geometric phase mechanism contribution in this performance augmentation.

Our evaluations are concerned with the generation of trajectories for the two-body (B2) and three-body (B3) systems with fully active hinge joints where not only does the center of mass coordinates of the systems on the plane but also the attitude coordinates of the rigid bodies comprising the systems have prescribed initial and final configurations. We also generate trajectories with equal starting and ending configurations for the rigid body and contrast the results of all systems with respect to a few cost functions detailed below. Discussion follows and attention is given to the multibody systems gain of performance over the rigid body system through the variation of the input structure and internal dynamics of the former systems. In like manner, other comparing functions involving the system barycenter trajectory and the thrusters effort dispensed are used to obtain a more complete measure of this performance gain.

2. MULTIBODY SYSTEM DYNAMICS

Let $\mathbf{r}_{cm} = (r_x, r_y) \in \mathbb{R}^2$ be the location of the center of mass of a planar, N-body system w.r.t. the inertial frame. For the i-th system body define the attitude angle θ_i relative to the inertial frame. Define the system mobile frame located at the center of mass whose angular orientation $\theta_{cm} \in \mathbb{S}^1$ is computed as a weighted average of the θ_i. The joint angles $\boldsymbol{\phi} = (\phi_1, \ldots, \phi_{N-1})$ solely determine the system shape and are the coordinates of the shape space B, where $B \subset \mathbb{R}^{N-1}$. We denote by q the system linear $(\mathbf{r}_{cm})$ and rotational $(\theta_{cm}, \boldsymbol{\phi})$ coordinates on the configuration space Q and by p the system translational and rotational conjugate momenta which yield an element z of the system n-dimensional phase space and parametrize it by (q, p). The multibody system dynamics represented in input-affine form gives, Souza and Maruyama (2011):

$$\dot{z} = f(z) + \sum_{k=1}^{m} g_k(q)u_k = f(z) + g(q)u, \quad (m < n) \tag{1}$$

where $f(z)$ and $\{g_1(q), \ldots, g_m(q)\}$ are the drift and the m input $\mathcal{C}^\infty$-vector fields, with input u. The m_t thruster forces f_i are located transversally on the centroid of each system body and propel the system everywhere on the plane. We allow bi-directional thruster actuation. The torques T_j drive $N-1$ joint angles. Notice that $m = m_t + (N-1)$. The structure of the m_t thruster input vector fields is

$$g_i = \begin{bmatrix} \mathbf{0}_{3\times 1} \\ \mathbf{0}_{(N-1)\times 1} \\ X_{v_x}(\theta_{cm}, \boldsymbol{\phi}) \\ X_{v_y}(\theta_{cm}, \boldsymbol{\phi}) \\ X_{p_\theta}(\boldsymbol{\phi}) \\ \mathbf{0}_{(N-1)\times 1} \end{bmatrix},$$

where $u_i = f_i$, for $i = 1, \ldots, m_t$, and the $N-1$ joint-torque vectors are written as

$$g_{m_t+1} = \begin{bmatrix} \mathbf{0} \\ 1 \\ 0 \\ \vdots \\ 0 \end{bmatrix}, \ldots, g_m = \begin{bmatrix} \mathbf{0} \\ 0 \\ 0 \\ \vdots \\ 1 \end{bmatrix} \Bigg\} (N-1)$$

where $\mathbf{0} = \mathbf{0}_{(N+5)\times 1}$ and $u_{m_t+j} = T_j$, for $j = 1, \ldots, N-1$. The B2 dynamical model is presented in the Appendix.

The RS, whose dynamics is detailed in the Appendix, has two thrusters located symmetrically on each side and at a distance d from the center of mass as shown in Fig. 2.

In the attempt to make a fair judgement and pinpoint the sources of possible gain in performance, we define the underactuated B3 system to have thrusters located exactly at the same place as those in the B2 system when both systems are extended with $\phi_i = 0$, see Fig 3. This rules out any dynamical advantage from thrusters location mismatch. A few comparison cases of the modified underactuated B3 system (with equivalent thruster locations to the B2 system) did show further significant J_{obj} and J_{PI} performance improvement over the B2 system and minor improvement of the trajectory. Hence, preliminary evaluations indicate that an extra elimination of kinematical restrictions enables further gain in performance.

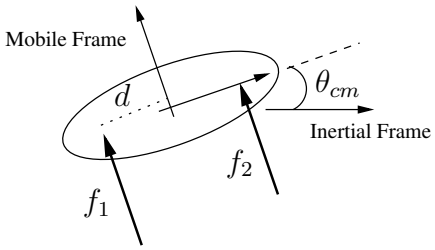

Figure 2. Rigid body or *reference* system.

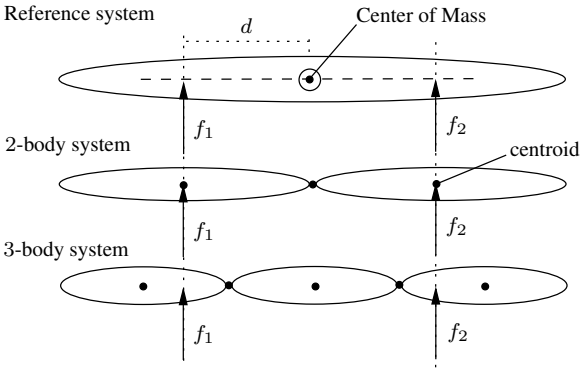

Figure 3. Position of thruster forces for the RS and the $2, 3$-body systems.

3. OPTIMAL CONTROL PROBLEM

Definition 3.1 (Optimal Control Problem - OCP) *The optimal control problem (OCP) consists of searching for the optimal trajectories $z^*(t)$ and controls $u^*(t)$ that minimize a specified objective function, satisfy the equations of motion (1) and (6), and the boundary and fixed final time T constraints which describe the system's final position and orientation.*

The objective function was chosen as a quadratic function on the system inputs, i.e., thruster forces f_i and joint torques T_j, and is given by

$$J_{obj} = \int \sum_{i=1}^{m_t} f_i^2 + w \sum_{j=1}^{N-1} T_j^2 dt \tag{2}$$

This choice of quadratic J_{obj} was made in order to avoid imposing input saturation (constraints) on the optimization problem and incorrectly infer conclusions about system behavior on arbitrary maximum input values for systems with different number of thrusters. We also encountered problems relative to numerical convergence with J_{obj} as a summation of absolute thruster forces.

Motivation for this specific choice of cost function relies on the fact that, for space robotic applications, for example, the energy needed for revolute joint actuation could benefit from renewable sources, such as the electricity generated from existing onboard solar panels. Some currently used energy sources for thrusters[1] are not renewable and electric propulsion technology is still in early stage of developement[2]. and, hence, the energy for the thrusting inputs are critical and should be minimized at the expense of increased effort for joint actuation.

The joint torques in (2) were weighted with penalty w. Different values for w verify how much the f_i can be minimized relative to the T_j. As expected, the higher the penalty w employed, the worse performance J_{obj} is obtained since the joint torques were minimized more intensely along with the thruster forces and less can be gained by exploiting the system internal dynamics performance.

In order to quantify the thruster effort and to compare the performance of the different topologies we make use of a metric, labeled performance index (PI), defined by truncating J_{obj} as

$$J_{PI} = \int \sum_{i=1}^{m_t} f_i^2 dt \tag{3}$$

The length of the trajectory described by the center of mass serves also as a performance metric for comparison

[1] Such as gas jets or burning of hydrazine derivatives.
[2] Which could still benefit from the optimization methods being discussed; specially when working near the operational performance limit.

between the different systems. This follows from

$$\Delta S = \int ds = \int_0^T \sqrt{v_x^2 + v_y^2} dt, \tag{4}$$

where (v_x, v_y) is the velocity of the system center of mass.

The boundary conditions are specified so that the systems leave the initial configuration from and arrive at the terminal configuration at rest ($p = 0$). The multibody systems initial and final shapes are constrained to mimic the RS with null joint angles ($\phi_j = 0$). This choice of boundary conditions allows for a direct comparison of the RS, B2, B3 systems: the multibody system are allowed to vary internal dynamics arbitrarily given they begin and finish the trajectories like the RS.

The RS and multibody systems have the same total mass m and moment of inertia I when the multibody system has $\boldsymbol{\phi} = 0$. The individual body mass m_i and inertia I_i of systems B2, B3 are computed according to

$$m_i = \frac{m}{N} \quad \text{and} \quad I_i \propto \frac{m}{N}\left(\frac{L}{N}\right)^2 \quad \Rightarrow \quad I_i = \frac{I}{N^3},$$

where N is the number of system bodies and L is the system characteristic length. This restricts the multibody systems to the similar geometric and inertial properties as the RS and applies to multibody systems which have mass distributed homogeneously with the length, e.g., system whose bodies are slender rods.

3.1 Numerical Implementation

Numerical computations are carried out with the PROPT commercial software package Rutquist and Edval (2010) which uses collocation methods to translate the optimal control problem into a Nonlinear Programming Problem (NLP) and solves the resulting NLP using a large-scale Sequential Quadratic Programming (SQP) engine. A Gauss discretization scheme was used to create collocation points. A mesh refinement study showed that 80 nodes resulted in a sufficiently fine mesh for the problem in question. The chosen trajectory final time T is of $10s$. Other numerical parameters include RS mass m of $10kg$, $d = 1m$, and $I = 10/3kgm^2$.

The terminal boundary conditions belong to a circle sector of radius $10m$ and centered at the origin of the inertial frame, which corresponds to the initial starting point for the RS, B2, B3 systems. We select some points on this circular sector as final system center of mass destinations. We extend the results of the above reference to include points parametrized by the angle α, which varies from 0° to -90° for the bidirectional case and from 0° to -180° for the unidirectional case, with increment values of 15°, as shown in Fig. 5(a). The unidirectional case mirrors this $1Q$ grid to the $4Q$. System final attitude $\theta_{cm}(T)$ were also selected from a set which begins at -180° and ends at $+180^\circ$, with increments of 15°. These, along with the restrictions of final system velocity, compose the system terminal boundary conditions. Additionally, we chose a objective function penalty w value of 0.1.

We employ two methods for generating the initial guess for optimal control u^* for the RS with bidirectional thrusters. The first consists in designing the necessary inputs for a piecewise rotation-translation-rotation trajectory. The first rotation simply aligns the RS attitude with the direction of the terminal center of mass position. The second, rotates the RS to coincide with the terminal RS attitude. The second method defines the guess for u^* as an interpolation of initial and terminal boundary conditions.

Using the above strategies as an initial guess for u^* in the unidirectional case proved to be, in general, unsuited for the RS optimal trajectory design since the optimization trials become unfeasible for many boundary conditions. In their stead, RS initial guess were obtained from the u^* of a previous, similar but simpler optimization trial of the many considered in the above terminal conditions parametrization. The first designed trajectory is the trivial RS translation and not rotation. The obtained optimal control u^* for the RS was then used as the initial guess for the optimal control u^* of multibody system models with either bidirectional or unidirectional thrusters.

3.2 Trajectory Generation Results

Of the 175 OCP trials for the bidirectional case and 325 OCP trials for the unidirectional case for each RS and multibody system, defined by the above mentioned boundary conditions, we summarize a few of the obtained results for the J_{PI} and ΔS functions for the RS, and the B2 and underactuated B3 systems in Table 2. Some values for the optimized functional J_{obj} are presented in Table 1.

Trajectories for one of the considered trials is depicted in Fig. 5(b). Comparison of the J_{PI} function for the bi and unidirectional cases for the RS, B2 and B3 systems can be seen in Fig. 4.

4. GENERAL COMMENTS AND DISCUSSION

The above results show that the B2 system enables lower J_{obj} and J_{PI} values for almost all considered boundary condition trials if compared to those obtained for the RS, Fig. 4. We remark that this observed gain of performance is

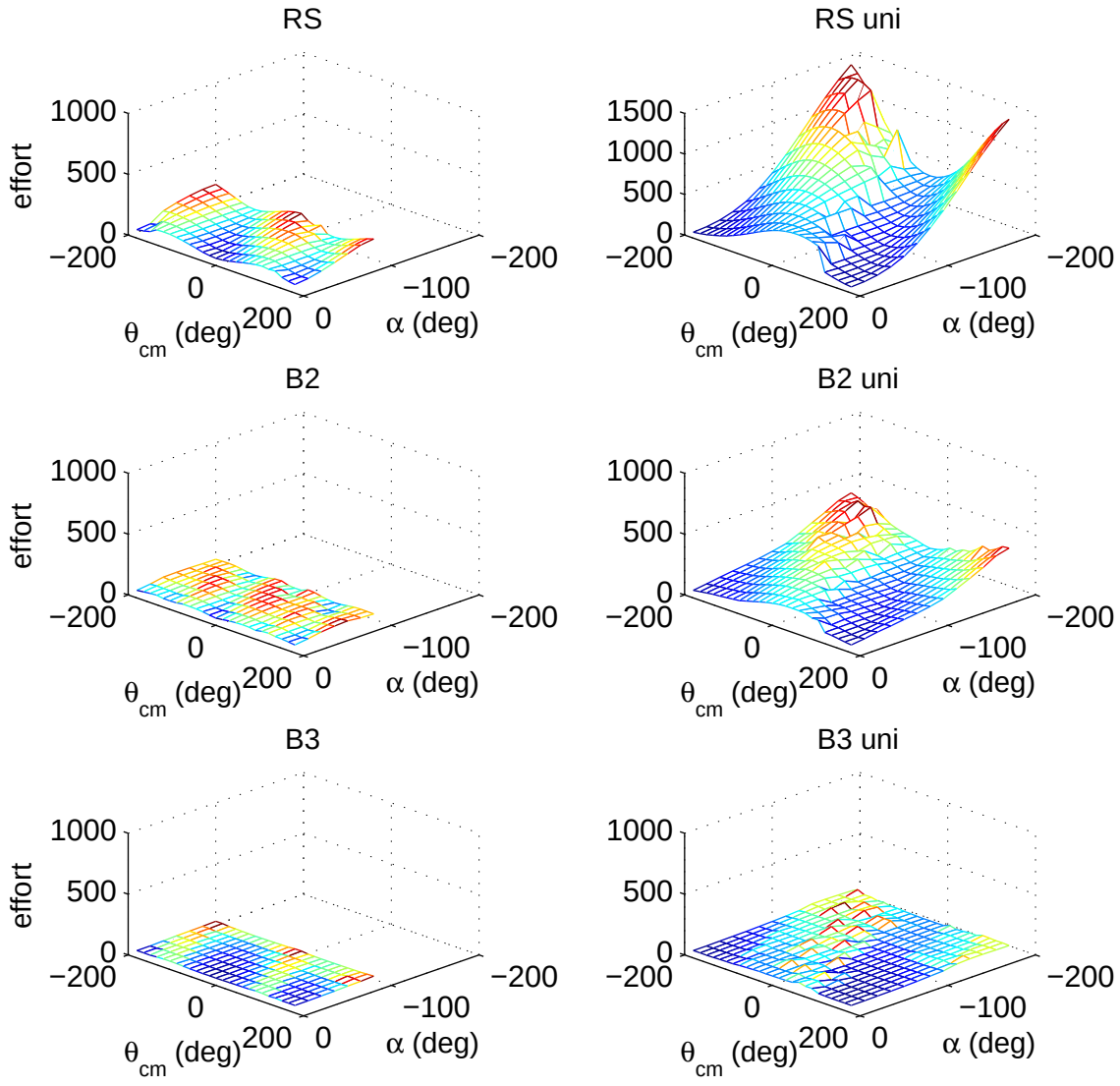

Figure 4. Rigid Body (RS) system J_{PI} performance and B2, B3 multibody systems gain of J_{PI} performance.

Table 1. Objective function J_{obj} for the B2, B3 systems.

Grid		**B2**		**B3**	
α	$\theta_{cm}(T)$	Bi	Uni	Bi	Uni
$-180°$	$-180°$	-	456	-	118
	$-90°$	-	297	-	98.7
	$0°$	-	192	-	85.5
	$90°$	-	297	-	104
$-135°$	$-180°$	-	313	-	125
	$-90°$	-	306	-	104
	$0°$	-	199	-	85.9
	$90°$	-	194	-	90.4
$-90°$	$-180°$	102	174	83.4	81.0
	$-90°$	76.6	353	70.7	103
	$0°$	89.0	218	82.9	106
	$90°$	76.6	110	70.7	69.6
$-45°$	$-180°$	108	115	71.6	66.6
	$-90°$	107	194	64.3	90.4
	$0°$	105	269	64.1	92.8
	$90°$	108	120	65.6	65.4
$0°$	$-180°$	63.5	63.7	61.0	60.9
	$-90°$	76.6	113	71.2	69.6
	$0°$	60.0	192	60.0	85.7
	$90°$	76.6	204	70.5	98.8

Table 2. Performance Index J_{PI} and trajectory ΔS functions for the bi and unidirectional RS, B2 and underactuated B3 systems.

		J_{PI}						ΔS					
Grid		Bi			Uni			Bi			Uni		
α	$\theta_{cm}(T)$	**RS**	**B2**	**B3**	**RS**	**B2**	**B3**	**RS**	**B2**	**B3**	**RS**	**B2**	**B3**
$-180°$	$-180°$	-	-	-	1464	413	101	-	-	-	17.66	11.39	10.02
	$-90°$	-	-	-	790	267	88.1	-	-	-	15.13	10.86	10.05
	$0°$	-	-	-	430	181	79.5	-	-	-	13.81	10.65	10.01
	$90°$	-	-	-	790	267	93.3	-	-	-	15.13	10.86	10.04
$-135°$	$-180°$	-	-	-	981	279	104	-	-	-	15.60	10.74	10.01
	$-90°$	-	-	-	834	261	91.7	-	-	-	15.09	10.86	10.09
	$0°$	-	-	-	414	178	80.0	-	-	-	12.83	10.49	10.05
	$90°$	-	-	-	418	176	82.6	-	-	-	12.99	10.39	10.02
$-90°$	$-180°$	217.0	93.3	76.2	463	157	75.1	10.32	10.04	10.00	12.58	10.16	10.05
	$-90°$	119.9	72.2	67.5	790	285	92.8	10.17	10.01	10.00	15.13	10.93	10.05
	$0°$	214.9	80.5	74.8	611	207	94.9	10.37	10.01	10.00	14.36	10.69	10.09
	$90°$	119.9	72.2	67.5	199	103	66.3	10.17	10.01	10.00	11.20	10.07	10.03
$-45°$	$-180°$	175.8	97.1	68.2	153	108	64.8	10.42	10.07	10.02	10.43	10.03	10.02
	$-90°$	114.4	101.9	63.2	418	176	82.6	10.29	10.03	10.02	12.99	10.39	10.02
	$0°$	121.4	100.5	62.7	530	235	82.4	10.25	10.02	10.01	14.19	10.99	10.02
	$90°$	149.6	105.3	64.0	186	113	63.6	10.38	10.38	10.02	10.33	10.07	10.02
$0°$	$-180°$	70.1	62.9	60.6	73.3	63.1	60.8	10.01	10.00	10.00	10.01	10.00	10.00
	$-90°$	119.9	72.2	67.6	199	102	66.4	10.17	10.01	10.00	11.20	10.08	10.03
	$0°$	60.0	60.0	60.0	430	181	78.3	10.00	10.00	10.00	13.81	10.65	10.00
	$90°$	119.9	72.2	67.4	464	173	87.3	10.17	10.01	10.00	13.11	10.64	10.05

solely attributed to the extra degree of freedom defined by the joint angle ϕ in the B2 system, given these systems possess the same number of thrusters and geometric and inertial properties, for $\phi = 0$, and thrusters are equally located on the same d-parametrized positions. A further gain in performance over the B2 system is achieved by the B3 system since an extra kinematic constraint is eliminated, enabling the use of two (ϕ_1, ϕ_2) joint angles for motion optimization. We remark that the trajectories optimized for the unidirectional thruster input proved to be a much more demanding task than

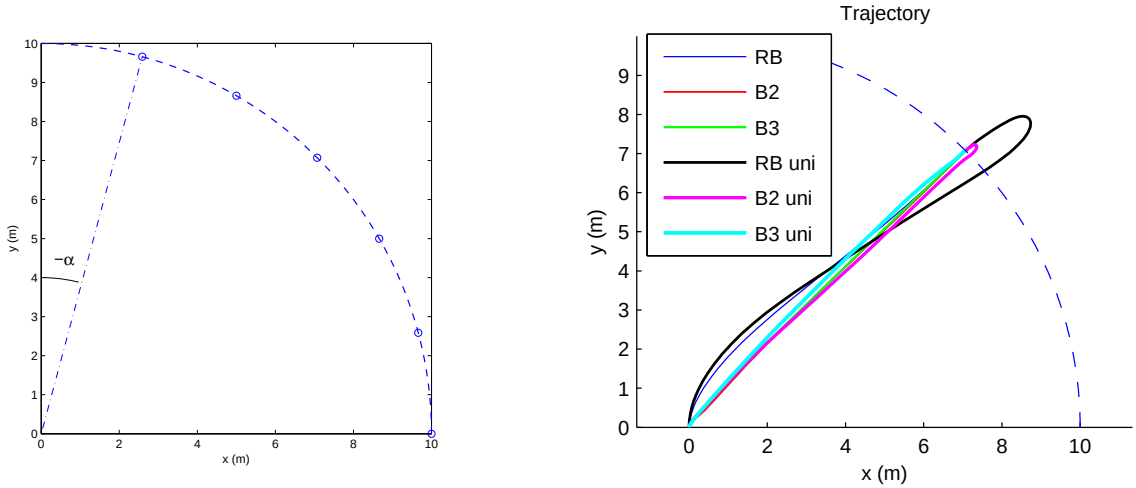

(a) Parametrization of systems terminal center of mass positions on the circular sector.

(b) Systems center of mass trajectories for $\alpha = -45°$ and $\theta_{cm} = -45°$.

Figure 5. System trajectories on the plane.

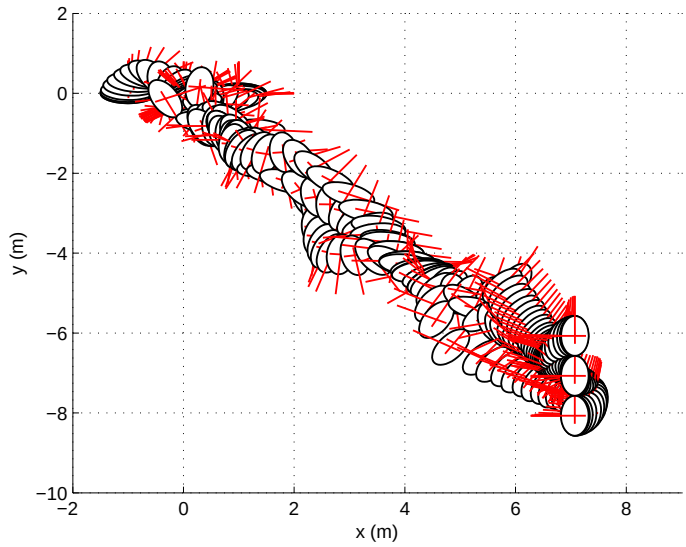

Figure 6. Snapshots of the B3 system along the trajectory on the plane for $\alpha = -135°$ and $\theta_{cm} = 90°$.

the corresponding bidirectional case, as can be seen from the greater effort (J_{PI}) values in Fig. 4 and from the required longer computational run times of the former. In many instances, the systems are required to turn around ($\theta_{cm} \rightarrow \pi$) in order to use the unidirectional thrusters to slow it down and reach the boundary condition at rest. Yet, while more demanding, the unidirectional case provided an even further gain of performance of the multibody systems over the RS. This can be observed in Fig. 4 by noting the greater distance of the B2,B3 functional surfaces from the RS in the graphs of the column on the right.

This improvement of performance seems to be achieved by way of two apparently distinct mechanisms: 1) through a more line-like trajectory, and 2) through the reduction of the system average angular displacement θ_{cm} along the trajectory. Notice that this statement is possible because multibody system drift translational and angular motions are decoupled. These dynamics, in contrast, become coupled through the input structure. This improvement tends to be more pronounced when the boundary conditions demand greater angular displacements.

The difference of center of mass displacements ΔS for the B2 and B3 systems in the bidirectional case is, in many examples, relatively insignificant and, thus, do not quantify a significant gain in performance. The displacement ΔS, however, proved to be a more useful and important metric to quantify the increase of performance when contrasting the B2 and B3 multibody system performance in the unidirectional case. Notice, from Table 2, that the B3 system is able to reach destination on a shorter CM trajectory and, thus, displacement ΔS than the corresponding displacement of the B2 system. Nevertheless, examination of the result tables indicate a progressive improvement, i.e., of shortening, of the center of mass trajectories for almost all considered cases with the RS, B2, and B3 systems, see Fig. 5(b). Additionally,

we observed that function values for greater penalty w are less optimal in terms of J_{PI} than those obtained with the lower values. This is because the greater the w, the smaller the performance transferred from force f_i driven dynamics to the torque T_j driven dynamics and, thus, multibody internal dynamics becomes less advantageous if compared to the RS dynamics.

We additionally observed a trend indicating that optimal control u^* implies expected optimal trajectories z^* for the considered design constraints even though a metric involving the trajectory was not contained in J_{obj}.

One other noteworthy advantage for the multibody system over the rigid body is that it is possible to maneuver the former even with a single thruster by making use of the geometric phases. Generally, the system motion in the bundle T^*Q with a cyclic motion in the base space B undergoes a shift in a direction not belonging to B called a phase shift or geometric phase, for zero total momentum. The magnitude of this shift is a function of the curvature of the connection, i.e. a measure of how curved a space is, and the area enclosed by the path the system dynamics performs in B. This shift is often given by an element of a group G, such as a rotation or translation group. Hence, changes in internal shape generate a shift in the system overall orientation.

The geometric phase can be computed by evaluating the following expression, Bloch (2003); Souza and Maruyama (2011):

$$\Delta\theta_{cm} = \exp\left(-\int_0^1 \mathcal{A}(\boldsymbol{\phi})\dot{\boldsymbol{\phi}}(t)dt\right) = -\int_\Gamma \mathcal{A}(\boldsymbol{\phi})d\boldsymbol{\phi} \tag{5}$$

where Γ is a closed path contour in the base or shape space, $\exp : \mathfrak{se}(2) \rightarrow SE(2)$ is the exponential map and the *mechanical connection* $\mathcal{A}$ which expresses the relationship between shape coordinates and system attitude is given by

$$\mathcal{A}(\phi) = \frac{\mathbb{J}(1, 2:N)}{\mathbb{J}(1,1)}$$

where $\mathbb{J}$ is the system inertia matrix and is function of shape $\boldsymbol{\phi}$. This feature is, however, not possible with the RS and B2 systems but only with multibody systems with 3 or more bodies. In fact, one can show even a single-thruster, 3-body system is accessible[3] from everywhere on the configuration space Q, irrespective of the position of this force on the system. One could devise an algorithm exploiting the system holonomy to generate trajectories, although not arbitrary, on the plane. The computed contribution geometric phases for the B3 system is depicted in Figs. 7 and 8. The surface gaps in figures mean the geometric phase and dynamics phase (obtained from $p_{\theta_{cm}}$) cancel each other out.

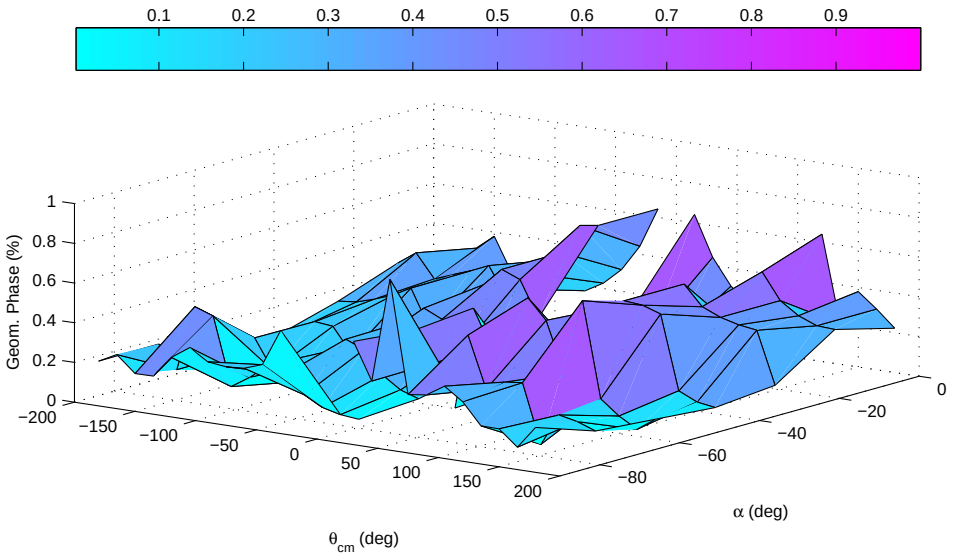

Figure 7. Geometric phases for the B3 system with bidirectional thrusters.

Although we believe that the J_{obj} along with ΔS and J_{PI} are reasonable metrics to quantify and compare system performance, nevertheless, a greater number of thrusters could contribute with greater angular momentum and with "turning" the system instead of using its internal dynamics to do so. On the other hand, the index J_{obj} does target f_i minimization (even if in the quadratic sense) and a careful tuning of the penalty w in J_{obj} is essencial in limiting much or, ultimately,

[3]Check Bloch (2003) and the references therein for a geometric approach to system accessibility.

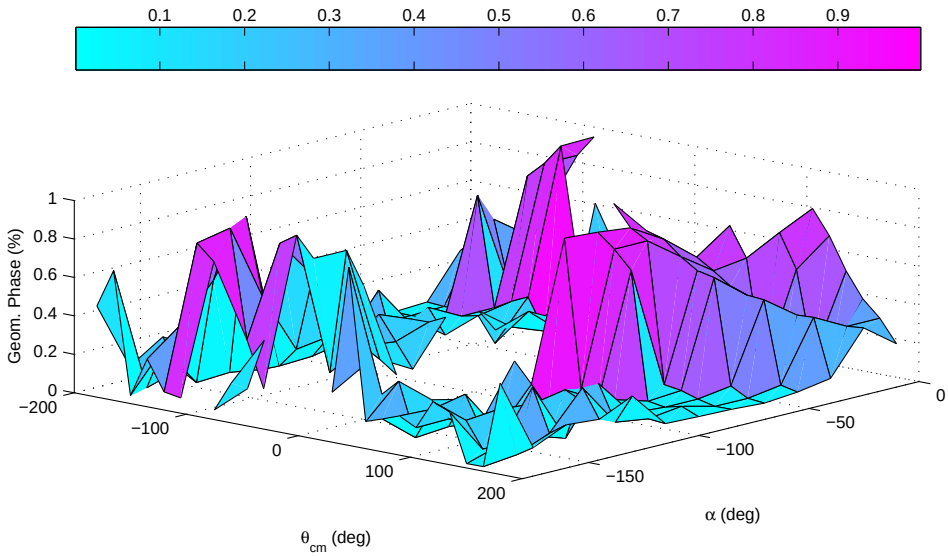

Figure 8. Geometric phases for the B3 system with unidirectional thrusters.

eliminating the f_i used for angular displacements. The underactuated B3 system did present a slightly worse performance than the fully actuated B3 system, as expected.

A recurrent problem encountered in our analysis, and surely a most important issue in numerical dynamical optimization problems, relates to determining whether the obtained numerical solutions are local or global. In general, for non-convex problems, it is difficult to ascertain that the problem won't get stuck at local minima. However, if we can determine that any local solution for the 2-body system outperforms the global solution for the RS, then working with the multibody system proves very advantageous. While determining whether the above RS optimum results is global or not is still a demanding task it surely is quite easier to guess how this optimum solution should be than the corresponding 2-body system optimum. We believe the obtained RS trajectories are close to, if not, the global optimal themselves.

The kinematically redundant multibody systems can achieve improved performance standards relative to the rigid body system performance, in particular compared to the RS considered. This, of course, depends on whether the multibody system can maneuver these extra d.o.f. accordingly and minimize a specific cost index (PI). Hence, the number of inputs present is decisive and underactuation, as observed with one considered version of the B3 system, can be detrimental to system overall performance.

5. CONCLUSIONS AND FUTURE RESEARCH

5.1 Conclusions

In this note we undertook the task of planning trajectories through numerical optimal control evaluations for a few multibody systems and compared the obtained results with those from the rigid body system for bidirectional and unidirectional thrusting capacity.

The gain of performance of the 2-body system over the rigid body system is due to an elimination, or "breaking", of kinematical constraints. The gain of performance of the 3-body w.r.t the 2-body can be explained by the possibility of turning the system, i.e., varying system overall attitude θ_{cm} through geometric phases and because of greater moment of thruster forces due to greater distance of point of action of forces to the center of mass.

5.2 Future Research

Current research efforts concentrate on expanding the above results to a more complete set of trajectories and verifying how close optimal results are to global, possibly through an analytical treatment. Attention will also be given to different objective functions that better convey objectivity in these comparison interests.

6. REFERENCES

Ackermann, M. and van den Bogert, A.J., 2010. "Optimality principles for model-based prediction of human gait". *Journal of Biomechanics*, Vol. 43, pp. 1055–1060.

Bloch, A.M., 2003. *Nonholonomic Mechanics and Control*, Vol. 24 of *Interdisciplinary Applied Mathematics*. Springer.
Dubowsky, S. and Papadopoulos, E., 1993. "The kinematics, dynamics, and control of free-flying and free-floating space robotic systems". *IEEE Trans. on Robotics and Automation*, Vol. 9, pp. 531–543.
Rui, C., Kolmanovsky, I.V. and McClamroch, N.H., 2000. "Nonlinear attitude and shape control of spacecraft with articulated appendages and reaction wheels". *IEEE Trans. on Automatic Control*, Vol. 45, pp. 1455–1469.
Rutquist, P.E. and Edval, M.M., 2010. *PROPT - Matlab Optimal Control Software*. Tomlab Optimization Inc., 1260 SE Bishop Blvd Ste E, Pullman, WA, USA - *http://tomdyn.com*.
Souza, E.C. and Maruyama, N., 2010. "Feedback linearization for stabilization of a class of mobile, multibody systems". 49^{th} *IEEE Conference on Decision and Control, Atlanta, USA*.
Souza, E.C. and Maruyama, N., 2011. "Hamiltonian dynamics and geometry of a class of mobile, multibody systems". 14^{th} *International Symposium on Dynamic Problems of Mechanics - DINAME, Sao Sebastiao-SP, Brazil*.

A Rigid Body and 2-Body System Models

Next, we proceed with the definition of a particular rigid body system.

Definition A.1 (Rigid Body System) *Let a rigid body with mass m and inertia I have two thrusters located symmetrically on each side and at a distance d from the center of mass. The system dynamics in inertial frame coordinates is given by*

$$\begin{aligned} \dot{x} &= p_x/m, \qquad \dot{p}_x = -\sin(\theta)f_1 - \sin(\theta)f_2 \\ \dot{y} &= p_y/m, \qquad \dot{p}_y = \cos(\theta)f_1 + \cos(\theta)f_2 \\ \dot{\theta} &= p_\theta/I, \qquad \dot{p}_\theta = d(f_2 - f_1). \end{aligned} \tag{6}$$

The equations of motion for the translational (trivial) dynamics of the 2-body system are:

$$\begin{aligned} \dot{r}_x &= \frac{p_x}{m}, \quad \dot{p}_x = \sin(\phi/2 - \theta_{cm})f_1 + \cos(\phi/2 + \theta_{cm})f_2, \\ \dot{r}_y &= \frac{p_y}{m}, \quad \dot{p}_y = \cos(\phi/2 - \theta_{cm})f_1 - \sin(\phi/2 + \theta_{cm})f_2. \end{aligned}$$

System rotational dynamics on $SE(2)$ are determined by

$$\dot{\theta}_{cm} = \frac{\partial H_0}{\partial p_{\theta_{cm}}} = \frac{p_{\theta_{cm}}(1/2)}{(\tilde{I} + K\cos(\phi))}, \quad \dot{p}_{\theta_{cm}} = -\frac{\partial H_0}{\partial \theta_{cm}} + \tau_p,$$

where $d_i = d$, $\tilde{I}_i = \tilde{I}$, $K = \epsilon d^2$, and $\tau_p = (d/2)(\cos(\phi) + 1)(f_2 - f_1)$. The reduced rotational dynamics are given by:

$$\dot{\phi} = \frac{\partial H_0}{\partial p_\phi} = \frac{2p_\phi}{(\tilde{I} - K\cos(\phi))}, \quad \dot{p}_\phi = -\frac{\partial H_0}{\partial \phi} + T = \frac{K\sin(\phi)}{4}\left(\frac{4p_\phi^2}{(\tilde{I} - K\cos(\phi))^2} - \frac{p_{\theta_{cm}}^2}{(\tilde{I} + K\cos(\phi))^2}\right) + T,$$

where T is the joint torque. The above expressions compose the drift f and input vector fields in (1). These equations of motion degenerate to the rigid body, RS dynamics when the two bodies are extended ($\phi = 0$) and at relative rest ($\dot{\phi} \equiv 0$).

Responsibility notice

The authors are the only responsible for the printed material included in this paper.